한국광물학회지 제 18 권 제 4 호 (2005년 12월)
J. Miner. Soc. Korea, 18(4), 249-257 (December, 2005)

A Study of Compressibility on a Natural Almandine Using Synchrotron Radiation

방사광을 이용한 천연산 알만딘의 압축성 연구

Gil Chan Hwang (황길찬) · Young-Ho Kim (김영호)*

Department of Earth and Environment Sciences and Research Institute of Natural Sciences,
Gyeongsang National University, Jinju 660-701, Korea
(경상대학교 지구환경과학과, 기초과학연구소)

ABSTRACT : Garnet is one of the major minerals down to the top of lower mantle approximately 660 km with spinel and pyroxenes. Garnet transforms into perovskite and corundum in the lower mantle, however its sequence is still in controversy. We measured the compressibility of a natural almandine at high-pressure up to 62 GPa using Mao-Bell type diamond anvil cell (DAC) at room temperature. Chemical formula of the specimen is $(Fe_{2.52}Ca_{0.21}Mg_{0.18}Mn_{0.12})Al_{2.23}Si_{2.97}O_{12}$. Results of this compression study are as follows: a = 10.775 Å, V = 1251.16 $Å^3$, D_x = 5.265 g/cm^3 at 62 GPa; bulk modulus is 156 GPa using Birch-Murnaghan equation of state (EoS) with a fixed K_0' of 4. This study would be the first time attempt accomplished with the high pressure DAC using synchrotron radiation at the Pohang Light Source (PLS) in Korea.

Key words : almandine, DAC, bulk modulus, EoS, synchrotron radiation, PLS

요약 : 석류석은 하부맨틀의 최상부인 약 660 km 깊이까지 올리빈, 휘석과 함께 주요한 구성광물 중의 하나이다. 석류석은 약 660 km를 지나 하부맨틀에서 페롭스카이트와 코런덤으로 상변이를 하는 것으로 알려져 있으나, 실험방법 및 상변이 깊이와 상변이 경로에 대해서 아직까지 논쟁의 대상이 되고 있다. 실험은 천연산 알만딘($(Fe_{2.52}Ca_{0.21}Mg_{0.18}Mn_{0.12})Al_{2.23}Si_{2.97}O_{12}$)에 마오-벨 타입의 다이아몬드 앤빌 기기를 이용하여 실온에서 62 GPa까지 압축실험을 시행하여 체적탄성계수를 결정하였다. 실험결과는 다음과 같다 : 62 GPa에서 격자상수 = 10.775 Å, 체적 = 1251.16 $Å^3$, X-선밀도 = 5.265 g/cm^3, 버치-머내한 상태방정식을 이용하여 계산한 체적탄성계수는 156 GPa이다(이때 K_0'는 4로 가정함). 본 연구는 포항가속기연구소의 방사광을 이용하여 시행한 국내 첫 고압실험결과이다.

주요어 : 알만딘, 다이아몬드앤빌기기, 체적탄성계수, 상태방정식, 방사광, 포항가속기연구소

*Corresponding Author (교신저자): yhkim@gsnu.ac.kr

INTRODUCTION

Garnet is represented as $A_3B_2(SiO_4)_3$, where A and B site refer to 8- and 6- coordinated cationic sites, respectively. The A sites are occupied by rather large divalent cation, whereas the B sites smaller trivalent cation. In a view of the A site concern, we may expect a fairly well-defined division of the garnet into those with easily interchangeable divalent ions such as Mg^{2+}, Fe^{2+}, Ca^{2+} and Mn^{2+}. Similarly, because of the limited substitution possible in the B site, it may be expected a separation of garnet into Al^{3+}, Fe^{3+}, and Cr^{3+} bearing constituents. These two trends are well marked and have given rise to a grouping of garnets into two series: pyralspite (Ca absent in A; B = Al) and ugrandite (A = Ca). Pyralspite group consists of pyrope ($Mg_3Al_2Si_3O_{12}$), almandine ($Fe_3Al_2Si_3O_{12}$) and spessartine ($Mn_3Al_2Si_3O_{12}$). On the other hand, grossular ($Ca_3Al_2Si_3O_{12}$), andradite ($Ca_3Fe_2Si_3O_{12}$), uvarovite, ($Ca_3Cr_2Si_3O_{12}$) and hydrogrossular ($Ca_3Al_2Si_2O_8(SiO_4)(OH)$) belong to the ugrandite group. The structure of garnet is such of body-centered cubic, space group Ia3d and atomic number of unit cell (Z) = 8.

Assuming the pyrolite as the average Earth upper mantle model, the mineralogy of this part would be as follows: olivine, orthopyroxene, clinopyroxene and garnet. Olivine, the most abundant mineral phase, has been up to now widely accepted that this mineral transforms to the modified spinel, and then to spinel, finally to perovskite plus magnesiowustite. These transformation sequences are responsible for the two major seismic discontinuities at 410 km and 660 km, respectively (Dziewonski and Anderson, 1981).

Garnet phase is stable in the wide range of pressure and temperature conditions. Geophysically, garnet phase sustains until approx. 660 km depth, which is the boundary between upper and lower mantle (Anderson, 1989). O'Neill and Jeanloz (1994) reported that garnet could coexist with aluminous perovskite up to about 50 GPa (about 1200 km depth), and proposed that iron in garnet could expand the garnet stability field to much higher pressure, compared with those in the iron-free systems.

Compared with magnesian garnet, the nature of phase transitions of iron-rich garnet is only poorly understood. Almandine, $Fe_3Al_2Si_3O_{12}$, is an iron -end member of pyralspite group in garnet phase. Almandine has been experimentally examined by several investigators, but their results are still in controversy. Liu (1975a, b) reported that almandine disproportionated into a mixture of stishovite and griphite (hydrophosphate garnetoid) at approx. 12 GPa, and further changed into wustite and unknown phase(s) at higher pressures. Kesson *et al.* (1995) suggested two alternatives that almandine disproportionates either into a mixture of wustites, corundum and stishovite or into a mixture of wustite, stishovite and $FeAl_2O_4$ (calcium ferrite structure), based on their diamond anvil cell (DAC) experiments at approx. 55～70 GPa. Conrad (1998) investigated perovskite phase does not form from almandine, and demonstrated almandine decomposes to oxides FeO, SiO_2, and Al_2O_3 rather than transforming to a perovskite- structured phase at lower mantle pressures. Akaogi *et al.* (1998) observed that almandine dissociates into a mixture of wustite, corundum and stishovite. The dissociation of almandine into the constituent oxides at 20～21 GPa shows a clear contrast to that of pyrope which decomposes into perovskite and corundum solid solutions at about 27 GPa.

Previous studies have been carried out mainly on the Mg-end member of pyrope (Recently, Irifune *et al.*, 1996; Kubo and Akaogi, 2000; Akaogi *et al.*, 2002). On the other hand, the Fe-end member of almandine has been lesser studied. In this study, we have carried out high-pressure experiments on a natural almandine, and determined the bulk modulus. This study would be the first time attempt accomplished with the DAC using synchrotron radiation (SR) at the Pohang Light Source (PLS) in Korea.

EXPERIMENTS

Sample Description

A natural almandine single crystal, which was

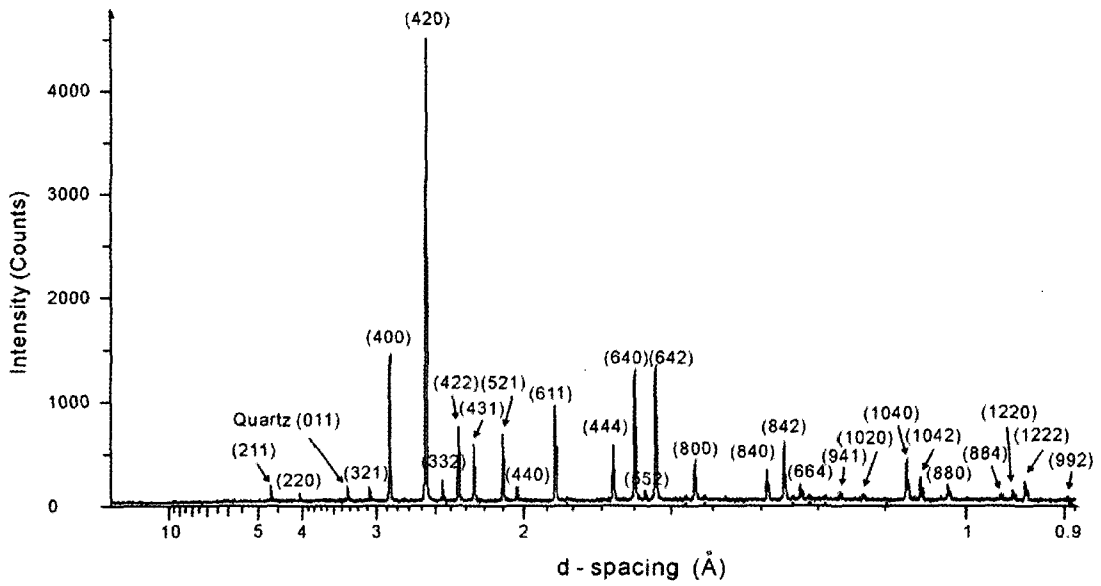

Fig. 1. ADXRD pattern of almandine with Miller index. 2θ ; $3\sim120^{\circ}$, sample rotation; 30 rpm. Other peaks does not exist except quartz (011). Intensity of almandine (420) is 4500 counts. Both almandine and quartz peak indices were assigned according to JCPDS 85-2498 and 85-0798, respectively.

embedded in the mica schist of the WARD collection (45E3120, No. 28) was separated and then crushed into pieces. These crystal pieces were cleaned using ultra-sonic cleaner and supposedly pure almandine specimens were carefully picked up manually under a stereo microscope. Pieces prepared through this procedure were grounded into a very fine polycrystalline powder.

X-ray diffraction (XRD) analysis was done on the powdered almandine using SIEMENS D5005 and XRD conditions were such that step-scan mode, 2θ angle for $3\sim120$ degree, voltage and current for 40 kV and 35 mA and Cu-K_{α} radiation with a graphite monochromator (Fig. 1). XRD pattern was indexed by JCPDS 85-2497. The d-spacings range from 4.730 to 0.898 Å, and the peak at 26.74 degree is assigned to quartz (011) (i.e., d-spacing of 3.3436 Å) from JCPDS 85-0798. Thus, in order to make clear their frac-tions, a quantitative analysis has been applied to XRD data using the Siroquant v2.5. Result in *Table 1 shows almandine* 96.2 ± 1.34 wt.% and quartz 3.8 ± 1.34 wt.% with X^2 of 2.19.

Electron Microprobe Analysis

Chemical composition of almandine was confirmed by electron probe micro-analyzer (EPMA) using CAMECA SX50 at the Korea Basic Science Institute (KBSI). The polished single crystal specimen of almandine was prepared for EPMA. Table 2 lists chemical composition of almandine we got in such ways. Each oxide was averaged from 10 measured data points : FeO 36.86%, SiO_2 36.23%, with Al_2O_3 20.95%, CaO 2.35%, MgO 1.44% and MnO 1.70%. On the basis of twelve oxygen atoms per formula, the chemical formula of almandine derived by the procedure of Klein and Hurlbut Jr. (1985) is the following: $(Fe_{2.52}Ca_{0.21}Mg_{0.18}Mn_{0.12})Al_{2.23}Si_{2.97}O_{12}$. Quartz in run #11 was neglected because of its very small amount.

High-pressure Experiment

Apparatus setup

X-ray measurements at high pressures were carried

Table 1. Result of quantitative analysis from XRD data

Phase	Weight (%)	Error
Almandine	96.2	1.34
Quartz	3.8	1.34

Chisquare (χ^2) = 2.19, using siroquant v2.5 (Rietveld method)

Table 2. Chemical composition of the natural almandine by EPMA

Oxides (wt.%)	Run 1~10 (Almandine)	Run 11 (Quartz)
SiO_2	36.229	98.514
Al_2O_3	20.953	0.733
MgO	1.436	-
CaO	2.347	-
TiO_2	0.049	0.03
FeO	36.86	0.314
MnO	1.701	-
Total	99.671	99.632

Divalent ions are such as Mg^{2+}, Fe^{2+}, Ca^{2+} and Mn^{2+}. This almandine includes the small amount of quartz.

out using synchrotron radiation at 1B2 beamline, available the white radiation, of PLS in the Pohang Accelerator Laboratory (PAL). PLS uses the synchrotron radiation in 2.5 GeV (Lee and Shin, 2002). Mixture of almandine and MgO powder in an indented gasket hole chamber at the inner DAC of Mao-Bell type was interfaced to the white SR using the Energy Dispersive X-ray Diffraction (EDXRD) technique. Fig. 2a in inlet describes this comment. Fig. 2 is the in-situ picture of the setup configuration and also shows the directions of both direct and diffracted beams which are indicated as 2θ schematically. Beam was collimated using stepping motor (SM) stage, which eliminates the unwanted XRD peaks from the gasket and other setup related materials by

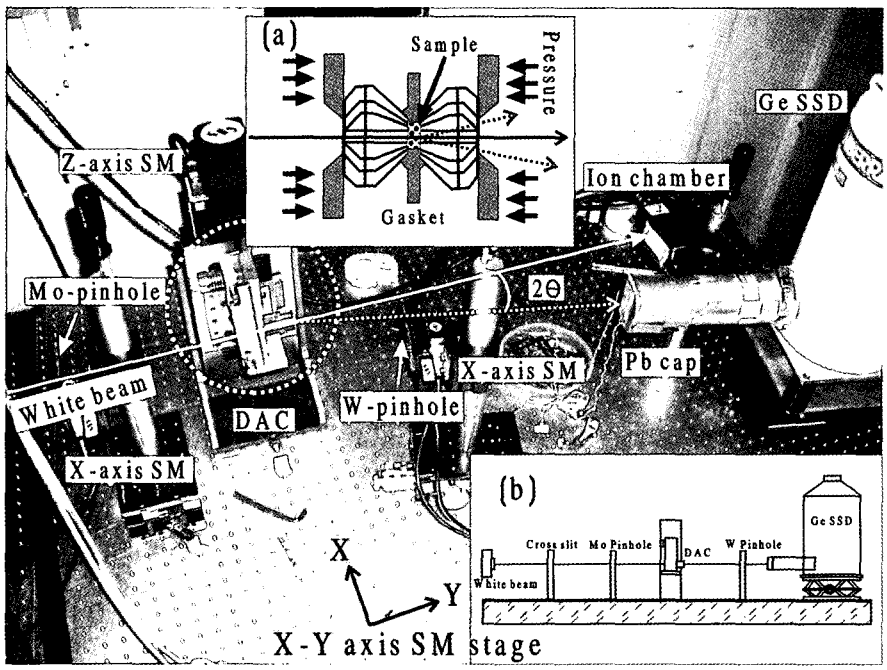

Fig. 2. Picture of experiment setup and schematic diagrams of beam directions within diamond anvil (a) and overall path (b). 2θ is the angle between incident white beam (solid line with arrow) and the diffracted to the Ge SSD (dotted line). Step motors (SM) were used for the collimations of pinholes to X-axis and of DAC to Z-axis. Beam size entering to DAC must be smaller (i.e., Φ177 μm) than gasket size (i.e., Φ235 μm) in order to get rid of the unwanted peaks through the pathway.

Table 3. XRD results and lattice parameters of almandine at the highest pressure (62 GPa)

I/Io[a]	E (keV)	d_{obs} (Å)	(hkl)	a (Å)	d_{cal} (Å)[b]	Phase[c]
90	21.77	2.702	(400)	10.809	2.694	al
100	24.47	2.404	(420)	10.751	2.409	al
10	26.70	2.203	(422)	10.794	2.200	al
10	30.32	1.940	(200)	3.880	1.940	MgO
5	33.74	1.744	(611)	10.748	1.748	al

[a]; Relative intensities were determined visually on spectrum.
[b]; The d-spacings were calculated on the basis of the following lattice parameter; a = 10.775 Å.
[c]; al stands for almandine.

Table 4. Lattice parameters, volume and density variations of almandine

P (GPa)	a (Å)	V (Å^3)	D (g/cm^3)
0	11.545	1538.839	4.281
3.311	11.445	1499.021	4.394
5.746	11.412	1486.280	4.432
10.841	11.333	1455.519	4.526
17.965	11.222	1413.390	4.661
25.782	11.123	1376.248	4.786
33.972	11.012	1335.181	4.934
41.732	10.921	1302.599	5.057
46.238	10.873	1285.452	5.125
51.341	10.837	1272.668	5.176
53.609	10.836	1272.446	5.177
59.906	10.781	1253.087	5.257
61.949	10.775	1251.155	5.265

P : pressure, a : lattice parameter, V : volume,
D : density

the X-ray path. So, the beam size must get to be smaller (i.e. Φ180 μm) than the gasket hole diameter of 235 μm. 2θ was set to be 12.11° to the Germanium solid state detector (Ge-SSD) (CANVERRA GL0210R, channel 4096), and this much 2θ is judged small enough to get the better resolution. Fig. 2b is the cross sectional view of the experiment setup with two pinholes (i.e., W and Mo plate with hole of 707 μm). These pinholes endeavor to prevent the dispersed beam from the scattering.

X-ray Measurements

MgO was used as the pressure medium as well as the pressure sensor (Vinet and Ferrante, 1987; Utsumi *et al.*, 1998; Singh *et al.*, 2004). Appropriate reasons of MgO selection for these purposes are such that there is a few overlapping of the diffracted peaks between MgO and almandine, especially between the strongest ones, and their analogs of physical properties each other (see Table 5), which would be described in detail below.

Sample chamber sustains its hydrostaticity by the immerged methanol and ethanol fluids (i.e., 4 to 1 in volume). This kind of experiment is fraught with difficulties arising from the small changes of specimen thickness under pressures and the need to maintain hydrostatic conditions, in order to remove all void space from the sample as well as to correct for the elasticity and the friction in the apparatus. The pressure was loaded step by step from 0.1 MPa (i.e., ~1 atmosphere) to 62 GPa at room temperature. Data collection time was assigned to be 20 minutes in live-time mode.

RESULTS AND DISCUSSIONS

High Pressure Results

A sequence of high pressure XRD spectrum is shown in Fig. 3. Almandine of Fig. 3a at 0.1 MPa shows totally 11 peaks of (321), (400), (420), (332), (422), (431), (440), (611), (444), (640) and (642) and moreover, together with the pressure medium (i.e., MgO) peaks of (200) and (220). Strongest almandine peak (420) situates at 15.63 keV and this peak would be used as a trace marker. Loading pressure to 26 GPa, the

Table 5. EoS parameters of almandine and MgO

Phase	EoS order	Parameter				P-V			Elasticity		f-F[c]	
		V_0	K_0	K_0'	K_0''	P	V^d	V/V_0	K(P)	K'(P)	Strain, f	Norm Pressure, F
Almandine	3	1538.839	156	4[a]	-0.0249	52.7274	1237.108	0.8039	347.4707	3.4099	0.0783	156.00
MgO	3	73.560	156[b]	4.7[b]	-0.0326	62.09076	58.4110	0.7941	417.282	3.9757	0.0831	169.610

Using EoS-fit v6.0 program (Angle, 2001), B-M; Birch-Murnaghan EoS, V; Volume, K; Bulk modulus, P; Pressure, a; fixed, b; Fei *et al.* (1990), c; f-F is stress-strain that Eulerian strain is $f_E=[(V_0/V)^{2/3}-1]/2$, normalized stress is defined as $F_E=P/3f_E(1+2f_E)^{5/2}$. d; values of high pressure experiment.

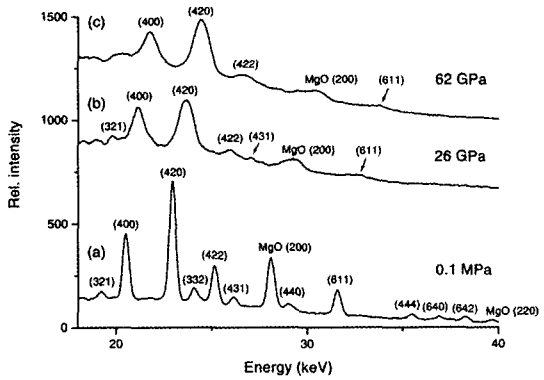

Fig. 3. Processes of the loading from 0.1 MPa to 62 GPa. (a) XRD pattern at 0.1 MPa (~1 atmosphyere), (b) Pressure of 26 GPa is equivalent to the mantle transition zone, (c) XRD pattern at the highest pressure of 62 GPa at present experiment. Only 5 peaks with MgO (200) are observable.

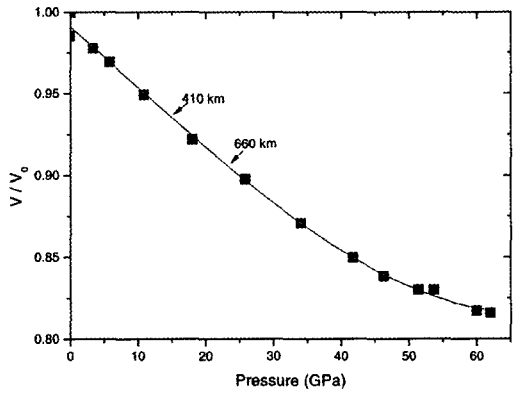

Fig. 4. Compression of the unit cell volume of almandine with pressure. Fitting line was drawn using Rorentz function. Pressure values which are equivalent to 410 km and 660 km, respectively are designated by arrows with numerics.

number of observable peaks becomes to 6 of (321) (400), (420), (422), (431) and (611) (Fig. 3b). At this pressure, only one MgO peak of (200) survives. Peak intensity during the loading process decreases gradually, and this might be due to the slim of sample thickness by the applied pressure. Continually, pressure was applied to almandine up to highest pressure of 62 GPa (Fig. 3c), and its XRD results are shown in Table 3, which only 4 sample peaks sustain with one MgO (200). In this Table, it is found that the difference between $d_{obs.}$ and $d_{calc.}$ of each peak is small enough to get the high level of confidence to the X-ray measurement at this highest pressure. Based on this reliance, we say new peak does not appear up to/and 62 GPa, therefore the phase transformation does not occur to any high pressure polymorph(s). Lattice parameter, volume and density variation of almandine are shown in Fig. 4 and Table 4.

According to the previous studies, pyrope transforms into perovskite and corundum phases above 23.5 GPa (Anderson, 1989). On the other hand, almandine does not transform at the mantle transition region which is equivalent to approximately 23.5 GPa, from high pressure and room temperature conditions (Akaogi *et al.*, 1998; Conrad, 1998). Our experimental result of the loading process up to 62 GPa agrees with those of Conrad's (1998), which shows the persistence of the unheated garnet to very high pressures. Almandine keeps stable up to about 12 GPa which is equivalent to 410 km depth and then

Table 6. Bulk moduli of various garnet phases

Composition	K_0 (GPa)	K_0'	Reference
$Mg_3Al_2Si_3O_{12}$	179±3	4.0	Hazen and Finger, 1989a
〃	175±1	4.5	Levien *et al.*, 1979
〃	171±3	1.8	Sato *et al.*, 1978
〃	190±6	5.45	Takahashi and Liu, 1970
〃	172.8	3.8	Leger *et al.*, 1990
$Mn_3Al_2Si_3O_{12}$	174.2	7.0	〃
$Fe_3Al_2Si_3O_{12}$	168±5	5.45	Takahashi and Liu, 1970
〃	175±7	1.5	Sato *et al.*, 1978
〃	156±0	4.0	This study
$Ca_3Al_2Si_3O_{12}$	168.4	6.1	Olijnyk *et al.*, 1991
〃	139±5	-	Hazen and Finger, 1978
$Ca_3Fe_2Si_3O_{12}$	159±2	4.0	Hazen and Finger, 1989b
$Ca_3Cr_2Si_3O_{12}$	162	4.7	Leger *et al.*, 1990
$Ca_3Al_2Si_3O_{12}(SiO_4)(OH)$	66±4	4.1	Olijnyk *et al.*, 1991

Upper part of the middle line is for pyralspite group and lower part for ugrandite group.

maintains its metastable phase up to 62 GPa. This might be due to the thermodynamic factor such as temperature which obstructs the interactions. For transition at matastable state, it must be true that important parameter is temperature. Almandine structure keeps to stable phase up to pressure which exceeds over the mantle transition zone.

Equation of State and Bulk Modulus

Generally, equation of state (EoS) relates to pressure (P), volume (V), temperature (T) of the material at given conditions. We have used the 3rd-order Birch-Murnaghan EoS (B-M EoS) (Birch, 1947):

$$P=\frac{3}{2}K_0(x^{-7}-x^{-5})[1-\frac{3}{4}(4-K_0')(x^{-2}-1)],$$

$$x=\left[\frac{V(T,P)}{V(T,0)}\right]^{1/3}$$

This is a "Finite strain EoS", and based on the assumption that the strain energy of a solid undergoing compression can be expressed as a Taylor series in the finite strain, *f*. The B-M EoS relies mainly on the Eulerian strain, $f_E=[(V_0/V)^{2/3}-1]/2$. EoS-fit starts a program to conform the B-M EoS to the acquired P-V data. As a result of EoS-fit using SAS v8.1, bulk modulus thus determined was 156±0 GPa where zero designates a very small standard deviation. EoS parameters of this natural almandine and MgO are given in Table 5. As mentioned above, MgO was used pressure sensor mainly as well as pressure medium. In addition to these roles, the reason MgO used is that strains (f) of almandine (i.e., 0.0783) and MgO (i.e., 0.0831) are similar each other (see Table 5), so that K_0 of each material happens to be same of 156 GPa. This means compressions of two materials proceed together constantly, and we can avoid the overlapping the XRD peaks at high pressures.

Comparing this value with the previously reported ones such as 168±5 GPa by Takahashi and Liu (1970) and 175±7 GPa by Sato *et al.* (1978) as the examples, the present one is rather low (Table 6). Bulk moduli of pyralspite group range usually from 171 to 190 GPa. However, those of ugrandite group shows the enormous range variations from 66 to 168 GPa (Table 6). Even if we put aside a hydrogrossular which shows 66 GPa due to the very compressible tetrahedral O_4H_4 structure, bulk modulus of an grossular in ugrandite group was reported as 139 GPa (Hazen and Finger, 1978 in Table 6). This value is lower than 168 GPa by almost 30 GPa of Olijnyk *et al.* (1991). As pointed out by this

study, probably Ca ion is judged to major cause of lower bulk modulus. However, part duties of other ions such as Mg^{2+} and Mn^{2+} substituted are beyond of this research.

However, Woodland *et al.* (1999) reported that a change in cation valence cannot explain the variation in bulk modulus between andradite or skiagite ($Fe^{2+}{}_3Fe^{3+}{}_2Si_3O_{12}$) and their Al-bearing analogs, grossular and almandine. Remaining the tetrahedral site environment more or less the same in all silicate garnets, it is the varying octahedral site that has the greatest direct influence on the bulk modulus.

SUMMARY

Garnet is regarded as one of the major minerals at the top of lower mantle. A natural almandine was compressed up to 62 GPa at room temperature using Mao-Bell type DAC interfaced to the white SR with EDXRD method. Within this high pressure range, lattice parameter and volume variations of an almandine are between 11.475 and 10.775 Å and between 1510.978 and 1250.984 $Å^3$, respectively. Accordingly X-ray density variation is 4.281 ~ 5.265 g/cm^3. Bulk modulus is determined to be 156±0 GPa. This natural almandine does not show any phase transition (s) so that almandine confirms its stability from 0.1 MPa to 62 GPa. This study would be the first time result for the Earth's material under high pressure using SR at PLS in Korea.

ACKNOWLEDGMENTS

Experiments at PLS were performed under the grant of both MoST and PLS (PLS apportionment numbers: 2003-3014-03 and 2004-1014-07). We are grateful to Dr. H.S. Yoon, 1B2 beam manager at PLS for his cooperation during high pressure works. Gaskets used for this study were provided by Dr. K.J. Kim of ADD. Prof. J.Y. Park of the Department of Information and Statistics at GSNU aided SAS manipulation.

REFERENCES

Akaogi, M., Ohmura, N. and Suzuki, T. (1998) High-pressure dissociation of $Fe_3Al_2Si_3O_{12}$ garnet: phase boundary by phase equilibrium experiments and calorimetry. Phys. Earth Planet. Int., 106, 103-113.

Akaogi, M., Tanaka, A. and Ito, E. (2002) Garnet-ilmenite-perovskite transitions in the system $Mg_4Si_4O_{12}$-$Mg_3Al_2Si_3O_{12}$ at high pressures and high temperatures: phase equilibria, calorimetry and implication for mantle structure. Phys. Earth Planet. Int., 132, 303-324.

Anderson, D.L. (1989) Theory of the Earth. Blackwell Scientific Publications, Oxford, pp.366.

Angel, R.J. (2001) Equations of state. In Hazen, R.M., Downs, R.T. (Eds.), "High-pressure, high-temperature crystal chemistry."-Reviews in Mineralogy and Geochemistry, 41, 35-60.

Birch, F. (1947) Finite elastic strain of cubic crystals. Phys. Rev., 71, 809-824.

Conrad, P.G. (1998) The stability of almandine at high-pressures and -temperatures, Properties of earth and planetary materials at high-pressure and -temperature. Geopys. Monogr., AGU, 101, 393-400.

Dziewonski, A.M. and Anderson, D.L. (1981) Preliminary Reference Earth Model. Phys. Earth Planet. Int., 25, 297-356.

Fei, Y., Saxena, S.K. and Navrotsky, A. (1990) Internally consistent thermodynamic data and equilibrium phase relations for compounds in the system MgO-SiO_2 at high-pressure and high temperature. J. Geophys. Res., 95, 6915-6928.

Hazen, R.M. and Finger, L.W. (1978) Crystal structures and compressibilities of pyrope and grossular to 60 kbar. Am. Mineral., 63, 297-303.

Hazen, R.M. and Finger, L.W. (1989a) High-pressure crystal chemistry of andradite and pyrope: revised procedures for high-pressure diffraction experiments. Am. Mineral., 74, 352-359.

Hazen, R.M. and Finger, L.W. (1989b) High-pressure and high-temperature crystal chemistry of beryllium oxide. J. Appl. Phys., 59, 3728-3733.

Irifune, T., Koizumi, T. and Ando, J. (1996) An experimental study of the garnet-perovskite transformation in the system $MgSiO_3$-Mg_3Al_2 Si_3O_{12}. Phys. Earth Planet. Int., 96, 147-157.

Kesson, S.E., Fitz Gerald, J.D., Shelley, J.M.G. and Withers, R.L. (1995) Phase relations, structure

and crystal chemistry of some aluminous silicate perovskites. Earth Planet. Sci. Lett., 134, 187-201.

Klein, C. and Hurlbut Jr. C.S. (1985) Manual of mineralogy, after JD Dana, John Wiley & Sons. NY, pp 596.

Kubo, A. and Akaogi, M. (2000) Post-garnet transitions in the system $Mg_4Si_4O_{12}$-$Mg_3Al_2Si_3O_{12}$ up to 28 GPa: phase relations of garnet, ilmenite and perovskite. Phys. Earth Planet. Int., 121, 85-102.

Lee, D.Y. and Shin, H.J. (2002) Introduction of synchrotron radiation science. Chungmungac, pp. 485.

Leger, J.M., Redon, A.M. and Chateau, C. (1990) Compressions of synthetic pyrope, spessartine and uvarovite garnets up to 25 GPa. Phys. Chem. Mineral., 17, 161-167.

Levien, L., Prewitt, C.T. and Weidner, D.J. (1979) Compression of pyrope. Am. Mineral., 64, 805-808.

Liu, L.G. (1975a) High-pressure reconnaissance investigation in the system $Mg_3Al_2Si_3O_{12}$-$Fe_3Al_2Si_3O_{12}$. Earth Planet. Sci. Lett., 26, 425-433.

Liu, L.G. (1975b) Chemistry and structure of high pressure phase of garnets rich in almandite. Nature, 255, 213-215.

Olijnyk, H., Paris, E., Geiger, C.A. and Lager, G.A. (1991) Compressional study of katoite ($Ca_3Al_2(O_4H_4)_3$) and grossular garnet. J. Geophys. Res., 96, 14313-14318.

O'Neill, B. and Jeanloz, R. (1994) $MgSiO_3$-$FeSiO_3$-Al_2O_3 in the Earth's lower mantle : Perovskite and garnet at 1200 km depth. J. Geophys, Res., 99, 19901-19915.

Sato, Y., Akaogi, M. and Akimoto, S. (1978) Hydrostatic compression of the synthetic garnets pyrope and almandine. J. Geophys. Res., 83, 335-338.

Singh, V. Gautam, A.K. and Sing, K.S. (2004) Analysis of a P-V-T relationship for MgO, Physica B, 352, 164-171.

Takahashi, T. and Liu, L.G. (1970) Compression of ferromagnesian garnets and the effect of solid solutions on the bulk modulus. J. Geophys. Res., 75, 5757-5766.

Utsumi, W., Weidner, D.J. and Liebermann, R.C. (1998) Volume measurement of MgO at high pressures and high temperatures. AGU, 101, 327-303.

Vinet, P. and Ferrante, J. (1987) Compressibility of solids. J. Geophys. Res., 92, 9319-9325.

Woodland, A.B., Angel, R.J., Koch, M., Kunz, M. and Miletich, R. (1999) Equations of state for $Fe_3^{2+}Fe_2^{3+}Si_3O_{12}$ "Skiagite" garnet and Fe_2SiO_4-Fe_3O_4 spinel solid solutions. J. Geophys. Res., 104, 20049-20058.

2005년 10월 8일 원고접수, 2005년 11월 7일 게재승인.